Randomized Phase III Trial Evaluating Sub-Cutaneous Rituximab for the First Line Treatment of Low-Tumor Burden Follicular Lymphoma: Results of a LYSA Study.

Supplemental methods

Pharmacokinetic data analysis was made using compartmental models and nonlinear mixed-effects modeling (population approach) using Monolix Suite 2020 (Lixoft®, Antony, France). The final model was used to compute values of area under the concentration curve (AUC) for each patient.

Structural model

Our model was based on a two-compartment model with first-order absorption, distribution, and elimination rates. As in previous studies, the effect of antigen mass on rituximab pharmacokinetics [1, 2] was implemented as a time-varying clearance component as in previous studies [3-5], which led to a better description of concentration-time data than target-mediated drug disposition (TMDD) model with irreversible binding approximation.[6-9] The model was implemented as follows:

$$\frac{dC_C}{dt} = In(t) - \frac{CL_0 + CL_1.exp(-k_{des}.t)}{V_1}.C_C - \frac{Q}{V_1}.C_C + \frac{Q}{V_2}.C_P$$

$$\frac{dC_P}{dt} = \frac{Q}{V_1}.C_C - \frac{Q}{V_2}.C_P$$

Where C_C and C_P are rituximab concentrations in central and peripheral compartments, respectively, In(t) is rituximab input function, V_1 andV_2 are central and peripheral volumes of distribution, respectively, CL_0 and Q are target-free systemic and intercompartment clearances, respectively, CL_1 is time-varying component of systemic clearance and k_{des} is first-order decline of CL_1. In addition, since rituximab was administered either by IV or subcutaneous (SC) route, SC bioavailability was estimated. Rituximab absorption kinetics following SC injection was described using a first-order absorption rate constant (k_a) as for most of SC monoclonal antibodies.[1]

Statistical models

Interindividual model. Pharmacokinetic parameters were assumed to follow a lognormal law, interindividual model was therefore exponential i.e. $\theta_i = \theta_{TV} . \exp(\eta_i)$, where θ_i is the estimated individual parameter, θ_{TV} is the typical value of the parameter and η_i is the random effect for the i^{th} patient. Values of η_i were assumed to be normally distributed with mean 0 and variance ω^2. The parameter F was assumed to follow a probit low since varies strictly between 0 and 1. Interindividual variances that could not be estimated properly were fixed to 0. In the present study, interindividual variances of V_1, CL_0, CL_1, V_2 and F. Interindividual variances of k_a, k_{des} and Q were not estimable and were therefore fixed to 0.

Residual model. Additive, proportional and mixed additive-proportional models were tested.

Model comparison and selection

Several structural models were tested, one-compartment and two compartment models with first-order distribution and elimination rate constants, then irreversible binding target-mediated elimination as in our previous works [6-9] and time-varying clearance as in previous other works. [3-5] Structural models were compared using Akaike's information criterion (AIC), defined as AIC = OFV + 2.p, where OFV is the value of the objective function and p is the number of model parameters to estimate. Interindividual and residual models were chosen by comparing nested models on the basis of the OFV tested using a likelihood ratio test (LRT). The two-compartment model with time-varying clearance led to a better description of concentration-time data (AIC=10504.28) compared to irreversible binding target-mediated elimination (AIC=10556.00), two-compartment model with first-order elimination rate (AIC=10572.70) or one-compartment model with first-order elimination rate (AIC=11519.22).

Model goodness of fit and evaluation

The goodness-of-fit was assessed for each model by plotting population-predicted (PRED) and individually predicted (IPRED) concentrations versus observed concentrations (DV) and IPRED and DV versus time. Population predictions were obtained using typical parameters, which include explained variability (i.e. population estimates and covariates), whereas individually predicted concentrations were obtained using individual parameters, which include both explained and unexplained (i.e. the random effects η_i for each PK parameter). In addition, the goodness-of-fit was evaluated by the distribution of residuals evaluated by graphical inspection of population (PWRES) and individual (IWRES) weighted residual distributions, visual predictive checks (VPC), and normalized prediction distribution errors (NPDE). These residuals should follow a standard normal distribution (i) to confirm a satisfactory description of the data using the model and (ii) to allow LRT tests (figure 1.)

Covariate analysis

Continuous covariates that were tested were baseline levels of alanine (ALAT) and asparagine (ASAT) aminotransferases, bilirubin (BILI), creatinine (CREAT), gamma-glutamyl trasferase (GGT), immunoglobulins (IGG), lactate deshydrogenase (LDH), white blood cell (WBC) and lymphocyte (LYM) counts, number of nodal sites, (NNS), number of nodal areas (NNA), median of maximal standardized uptake value obtained by PET-CT (SUV), body weight (BW), body surface area (BSA) and height (HT). All of these covariates, except for NNS and NNA were coded as a power function and centered to their median. Categorical covariate was sex, with females taken as a reference. The influence of each covariate on statistical models was based on the During univariable step, the association of each covariate was tested. Each covariate showing a significant influence ($\alpha < 0.1$) was kept for multivariable step. During the multivariable step, a forward and backward stepwise selection process was performed, where covariates were added and then removed during forward and backward steps, respectively. Covariates which

inclusion ($\alpha<0.05$) in forward or which exclusion ($\alpha<0.01$) during backward steps were retained in the final model.

The final covariate model presented (table 1) increased V_1 with BSA ($p=4.19.10^{-6}$) and HT ($p=0.00041$), increased or decreased CL_1 with BSA ($p<10^{-16}$), and NNA ($p=0.0027$), or CREAT ($p=0.01$), respectively, increased CL_1 with NNA ($p=0.0055$) and increased V_2 with BSA ($p=7.2.10^{-7}$).

The final statistical model was therefore:

$$F = 0.76.e^{\eta_{F,i}}$$

$$V_1 = 3.5.\left(\frac{BSA}{1.87}\right)^{0.74}.\left(\frac{HT}{169}\right)^{1.4}.e^{\eta_{V1,i}}$$

$$CL_0 = 0.21.\left(\frac{BSA}{1.87}\right)^{2.0}.\left(\frac{CREAT}{70}\right)^{-0.27}.e^{0.027.NNA}.e^{\eta_{CL0,i}}$$

$$CL_1 = e^{0.090.NNA}.e^{\eta_{CL1,i}}$$

$$V_2 = 3.5.\left(\frac{BSA}{1.87}\right)^{1.6}.e^{\eta_{V0,i}}$$

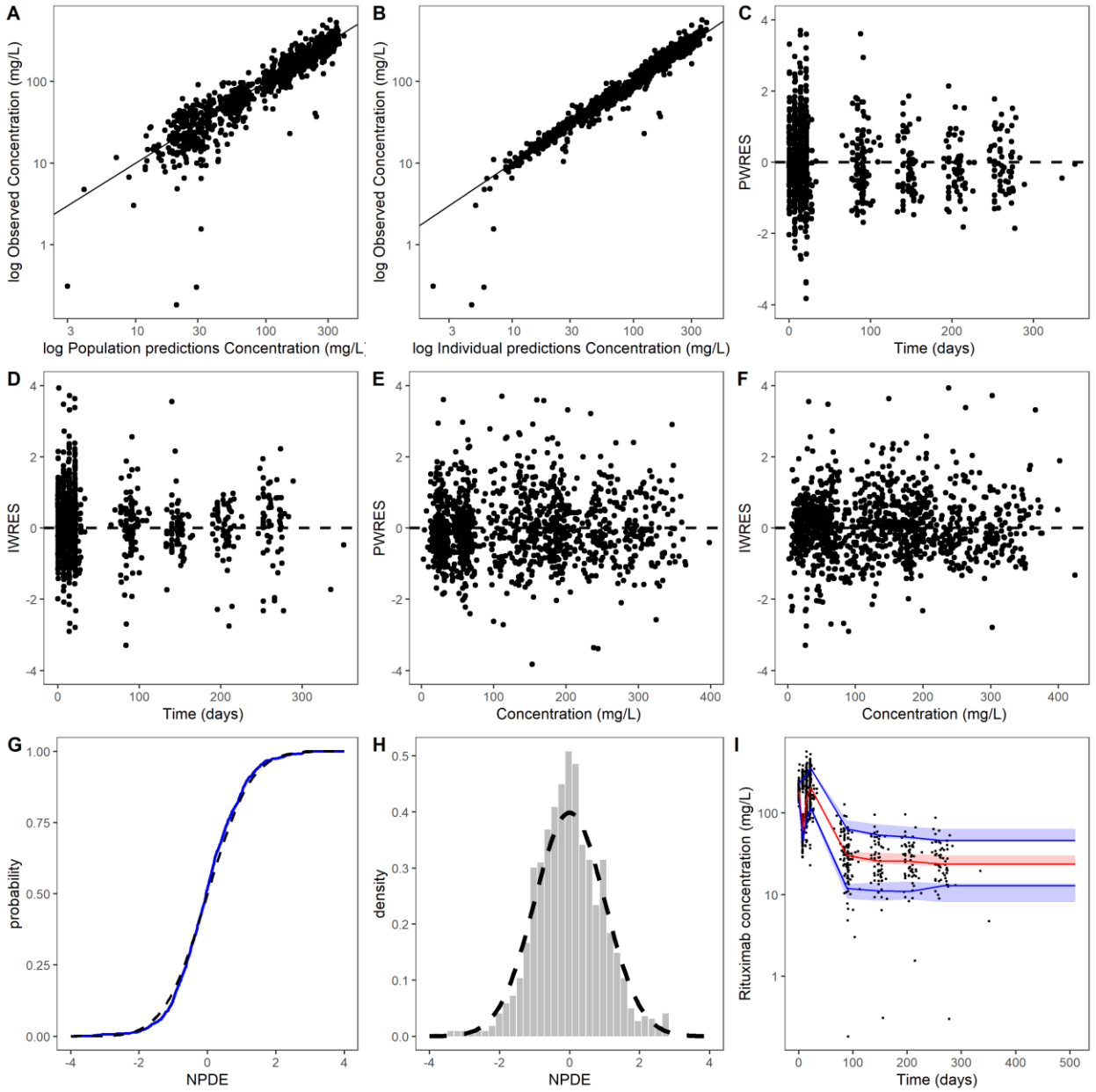

Supplemental Figure 1. Goodness-of-fit charts of the PK model. Legends: (A) Observed rituximab concentration vs population prediction (PRED); and (B) observed rituximab concentration vs individual prediction (IPRED). Solid black line represents the identity line. (C) Population (PWRES); and (D) Individual-weighted residuals (IWRES) vs time; and (E) Population; and (F) Individual-weighted residuals (IWRES) vs individual prediction; (G) Normalized prediction distribution error (NPDE) distribution vs. Gaussian density; and (H) probability. Dashed line is theoretical Gaussian distribution; (I) Visual predictive check (VPC) plot. Observed (black circles) concentrations, empirical (continuous lines) percentiles (from bottom to top: 10%, 50% and 90% percentiles) and prediction interval (from bottom to top: 10%, 50% and 90% prediction intervals).

Supplemental Table 1. Pharmacokinetic parameter estimates for base and final models.

Parameter	Unit	Model			
		Base model		Final model	
		Estimate	RSE%	Estimate	RSE%
k_a	day^{-1}	0.21	6.3	0.22	12
F	–	0.80	3.1	0.76	3.7
V_1	L	3.5	2.1	3.5	2.4
CL_0	$L.day^{-1}$	0.25	3.5	0.21	5.2
CL_1	day^{-1}	0.068	30	0.10	28.0
k_{des}	day^{-1}	0.029	20	0.056	13.0
V_2	L	3.9	4.6	3.5	6.4
Q	$L.day^{-1}$	0.76	2.1	0.69	18.0
BSA_V_1	–	–	–	0.74	22
HT_V_1	–	–	–	1.4	29
BSA_CL_0	–	–	–	2.0	9.5
NNA_CL_0	–	–	–	0.027	33
CREAT_CL_0	–	–	–	-0.27	39
NNA_CL_1	–	–	–	0.090	36
BSA_V_2	–	–	–	1.6	16
ω_F	–	0.44	17	0.41	14
ω_{V1}	–	0.17	10	0.097	18
ω_{CL0}	–	0.29	8.0	0.21	7.9
ω_{CL1}	–	0.93	19	0.53	15.0
ω_{V2}	–	0.25	12	0.11	46
σ_{add}	mg/L	2.2	18	2.2	18
σ_{prop}	–	0.16	2.9	0.16	2.9

Legends. RSE: relative standard error, k_a: first-order absorption rate constant, F: bioavailability, V_1 andV_2: central and peripheral volumes of distribution, respectively, CL_0 and Q: target-free systemic and intercompartment clearances, respectively, CL_1: time-varying component of systemic clearance, k_{des} is first-order decline of CL_1, ω: interindividual standard deviation, σ: residual standard deviation.

References

1. Bensalem A, Ternant D. Pharmacokinetic Variability of Therapeutic Antibodies in Humans: A Comprehensive Review of Population Pharmacokinetic Modeling Publications.- *Clin Pharmacokinet*; 2020; Online ahead of print.
2. Ternant D, Azzopardi N, Raoul W, et al. Influence of Antigen Mass on the Pharmacokinetics of Therapeutic Antibodies in Humans.- *Clin Pharmacokinet*; 2019; 58: 169-87.
3. Assouline S, Buccheri V, Delmer A, et al. Pharmacokinetics and safety of subcutaneous rituximab plus fludarabine and cyclophosphamide for patients with chronic lymphocytic leukaemia.- *Br J Clin Pharmacol*; 2015; 80: 1001-9.
4. Gibiansky E, Gibiansky L, Chavanne C, et al. Population pharmacokinetic and exposure-response analyses of intravenous and subcutaneous rituximab in patients with chronic lymphocytic leukemia.- *CPT Pharmacometrics Syst Pharmacol*; 2021; 10: 914-27.
5. Jamois C, Gibiansky E, Gibiansky L, et al. Quantitative Clinical Pharmacology Supports the Bridging From i.v. Dosing and Approval of s.c. Rituximab in B-Cell Hematological Malignancies.- *Clin Pharmacol Ther*; 2021; 110: 1261-72.
6. Bensalem A, Cartron G, Specks U, et al. The Influence of Underlying Disease on Rituximab Pharmacokinetics May be Explained by Target-Mediated Drug Disposition.- *Clin Pharmacokinet*; 2022; 61: 423-37.
7. Bensalem A, Mulleman D, Paintaud G, et al. Non-Linear Rituximab Pharmacokinetics and Complex Relationship between Rituximab Concentrations and Anti-Neutrophil Cytoplasmic Antibodies (ANCA) in ANCA-Associated Vasculitis: The RAVE Trial Revisited.- *Clin Pharmacokinet*; 2020; 59: 519-30.
8. Ternant D, Monjanel H, Venel Y, et al. Nonlinear pharmacokinetics of rituximab in non-Hodgkin lymphomas: A pilot study.- *Br J Clin Pharmacol*; 2019; 85: 2002-10.
9. Tout M, Gagez AL, Lepretre S, et al. Influence of FCGR3A-158V/F Genotype and Baseline CD20 Antigen Count on Target-Mediated Elimination of Rituximab in Patients with Chronic Lymphocytic Leukemia: A Study of FILO Group.- *Clin Pharmacokinet*; 2016; 2016: 25.